Validation of GOES-16 ABI Reflective Solar Band Calibration through Reanalysis and Comparison with Field Campaign Data

Xi Shao[1], Xiangqian Wu[2], Changyong Cao[2], Sirish Uprety[3]， Fangfang Yu[1], Haifeng Qian[1], Frank Padula[4], Aaron Pearlman[4], Taeyoung Choi[1], Brent Bartlett[4]， Jason Casey[4]
[1]Earth Resource Technology, Inc., Laurel, MD, USA,
[2] NOAA/NESDIS/STAR, College Park, MD
[3] University of Maryland, College Park, MD
[4]GeoThinkTank LLC., Washington DC

ABSTRACT

The Advanced Baseline Imager (ABI) is a critical instrument onboard GOES-16 which provides high quality Reflective Solar Bands (RSB) data though radiometric calibration using onboard solar diffuser. Intensive field campaign for post-launch validation of the ABI L1B spectral radiance observations was carried out during March-May, 2017 to ensure the SI traceability of ABI. In this paper, radiometric calibrations of the five RSBs of ABI are evaluated with the measurements by Airborne Visible/Infrared Imaging Spectrometer (AVIRIS-NG) onboard the high-altitude aircraft ER2. The ABI MESO data processed by the vendor with ray-matching to AVIRIS-NG during the field campaign was compared with the AVIRIS-NG measurements for radiometric bias evaluation. Furthermore, there were several implementations and updates in the solar calibration of ABI RSBs which resulted in different versions of detector gains and nonlinear calibration factors. These calibrations included the calibration by the operational ground processing system, by vendor and the calibration with updated nonlinear calibration factor table for striping mitigation and accounting for the integration time difference between solar calibration and Earth view. The North-South Scan (NSS) field campaign data of ABI were re-processed with these calibration coefficients to quantitatively evaluate the detector uniformity change. The detector uniformity difference are traced back to the difference in the implementation of the solar calibration.

Keywords: GOES-16 ABI, Radiometric Calibration, Radiometric Bias, AVIRIS-NG, North-South Scan, Airborne Field Campaign

1. INTRODUCTION

Being the first satellite in the next generation of geostationary Earth-observing systems, GOES-16 (previously known as GOES-R) was successfully launched on Nov. 19, 2016 [1-3]. The Advanced Baseline Imager (ABI) onboard GOES-16 provides high quality Reflective Solar Bands (RSB) data though radiometric calibration using onboard solar diffuser. The radiometric uncertainty for ABI RSB channel (CH01-CH06) is required to be within 5%. Prelaunch calibration of ABI has SI traceability to NIST calibrated using transfer integrating sphere & FEL lamp. Intensive field campaign for post-launch validation of the ABI RSB L1B spectral radiance observations was carried out with AVIRIS-NG (Airborne Visible InfraRed Imaging Spectrometer - Next Generation) instrument onboard NASA ER-2 High-Altitude Airborne Science Aircraft during March-May, 2017 [4-6] to ensure the post-launch SI traceability of ABI.

AVIRIS-NG has been developed following the legacy AVIRIS to provide continued access to high signal-to-noise ratio (SNR) imaging spectroscopy measurements in the solar reflected spectral range [7-8]. It measures the wavelength range from 380 nm to 2510 nm with 5 nm sampling (480 channels). Spectra of AVIIRS-NG are measured as images with 600 cross-track elements at spatial sampling of 1.0 ± 0.1 mrad. AVIRIS-NG has better than 97% cross-track spectral uniformity and >= 97% spectral IFOV uniformity. AVIRIS-NG has onboard calibrator source and maintains < 3% uncertainty with SI traceability to NIST via FEL Lamp. It has a FOV of 34 degrees. The spatial swath of AVIRIS-NG is ~11 km with spatial resolution of ~20 m at an altitude of 20 km.

Earth Observing Systems XXIII, edited by James J. Butler, Xiaoxiong (Jack) Xiong, Xingfa Gu, Proc. of SPIE Vol. 10764, 107640I · © 2018 SPIE · CCC code: 0277-786X/18/$18 · doi: 10.1117/12.2323024

In this paper, comparison between ABI and AVIRIS-NG radiometric measurement was performed. The focus is on the comparison between GOES-16 ABI RSB channel and AVIRIS-NG data collected during the field campaign on Mar. 28, 2017. Using ABI MESO scene observation on Mar. 28, 2017 as an example, we show detailed analysis of ABI and AVIRIS-NG radiance difference for the RSB channels. Overall radiometric performance of ABI RSB channel in comparison with AVIRIS-NG and LEO SNPP VIIRS measurements are discussed.

Furthermore, there were several implementations and updates for the solar calibration of ABI RSB channel which resulted in different versions of detector gains and nonlinear calibration factors. These calibrations include the calibration by the operational ground processing system, by vendor, *i.e.* Pleiades, and calibration with updated nonlinear calibration factor table for striping mitigation and accounting for the integration time difference between solar calibration and Earth view. Reanalysis was performed on the North-South Scan (NSS) data collected during the ABI field campaign using various calibration algorithms. Using ABI CH01 as an example, the variation in detector uniformity was evaluated and traced back to the difference in the implementation of the solar calibration.

2. DATA COLLECTION DURING FIELD CAMPAIGN

GOES-16 ABI has six RSB channels covering spectral range from 0.47 um to 2.25 um with spatial resolution of 1.0, 0.5, 1.0, 2.0, 1.0, 2.0 km for ABI CH01-06, respectively. The ABI data collection during the field campaign on Mar. 28, 2017 was executed under Timeline 25 scheduling with the GOES-16 nadir checkout location being at -89.5 W. Each Timeline 25 mode has 5-minute duration. During Timeline 25 mode of ABI, both ABI MESO and NSS were performed.

Each ABI MESO scan consists of two swaths covering the Sonoran Desert where simultaneous air-borne measurements were performed during the field campaign. Such MESO scan was repeated ten times during each Timeline 25 operation and data were collected for each of the ABI channel. The ABI NSS was performed by fixing the ABI East/West scan mirror angle while rotating the ABI North/South scan mirror.

On Mar. 28, 2017, the targeted field campaign location is placed over Sonoran Desert with ~90-minutes coordinated data collection. Figure 1 show the ground track of AVIRIS-NG instrument onboard ER-2 on Mar. 28, 2017. About 8 circular flight ground track were carried out over the region of Sonoran desert to ensure the view geometry of AVIRIS-NG matched that of ABI over the target region. Figure 2 shows the sample ground Track of ABI NSS during Timeline 25 for Channel #1-2 around UT 19:25 on Mar. 28, 2017. AVIRIS-NG scans as far as 34 degree off-nadir, nadir, thus with the addition of a ~33 degree bank angle from the ER-2 enabled a match of the ABI view geometry over the target location.

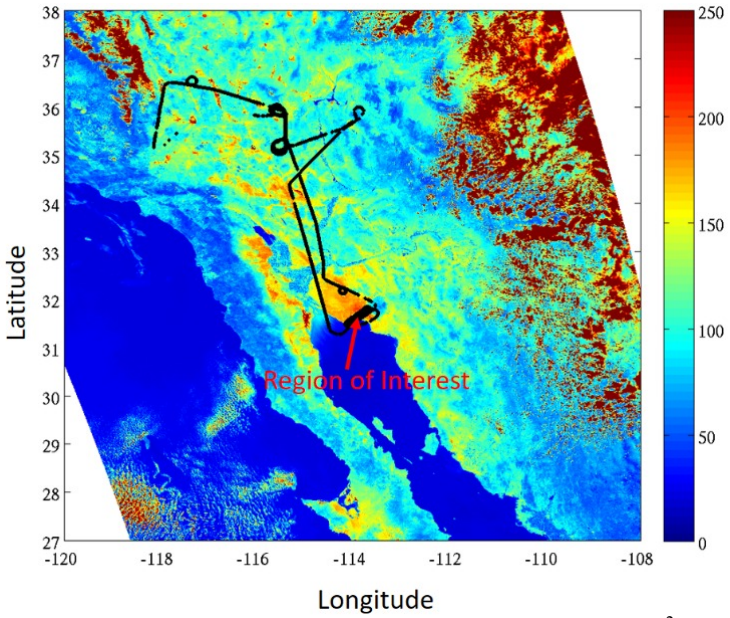

Figure 1: Ground track of ER-2 (black line) overlaid on GOES-16 CH02 radiance (W/m^2-sr-um) image during the field campaign on Mar. 28, 2017.

The ABI Timeline 25 special scan data collected during field campaign need to be calibrated and navigated. The ABI MESO data used in this report were specially processed by vendor, *i.e.* Pleiades version. In the Pleiades version of reprocessed ABI data, solar calibration to derive detector gain factor, processing the raw data to radiance data and imagery navigation were all performed by the ABI vendor. Figure 3 shows example of radiance map from AVIRIS-NG data (left) and ABI-Pleiades data (right) for ABI CH02 on Mar. 28, 2017. The AVIRIS-NG hyperspectral data has been convolved with the ABI spectral response function (SRF) for ABI CH02. In such as way, the AVIRIS-NG effective spectral radiance over ABI CH02 can be calculated using its SRF. Note that AVIRIS-NG data was accumulated over ~an hour on Mar. 28 and the ABI data is from one snapshot of MESO scene scan. The overall radiance maps derived from AVIRIS-NG and ABI measurements are consistent. The difference between the two panels are mainly due to several factors such as different sensor view angle and data collection over ~60-minute period for AVIRIS-NG vs. snapshot for ABI. More precise radiometric comparison between ABI and AVIRIS-NG measurements require the matching in view geometry and time between these two sensors.

The NSS mode is designed to make the detector of each ABI channel sequentially scan through the same location on Earth and to evaluate the detector uniformity for each ABI channel (Figure 2). Since the detector arrays for different channels are located at different location on focal plan module, during each NSS, only the detector array for selected channel can scan through the target location on Earth while the detectors of all other channels are away from the target location. Therefore, during the ABI Timeline 25, it was designed that the NSS scans over the target location when Swath number = Channel number. During the 5-minute ABI Timeline 25 mode, the NSS were repeated four times for each ABI channel. In this paper, ABI NSS data was used to evaluate the performance of detector uniformity improvement with updated solar calibration algorithm.

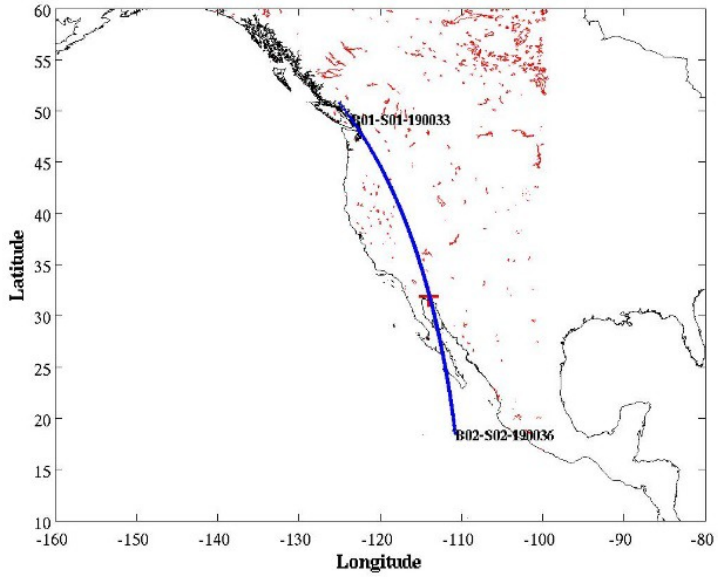

Figure 2: Ground Track of ABI NSS during Timeline 25 for Channel #1-2 around UT 19:25 on Mar. 28, 2017. The ABI NSS during Timeline 25 is designed to overpass the target location for Swath number = Channel number. The red "+" sign marks the target desert location for the NSS.

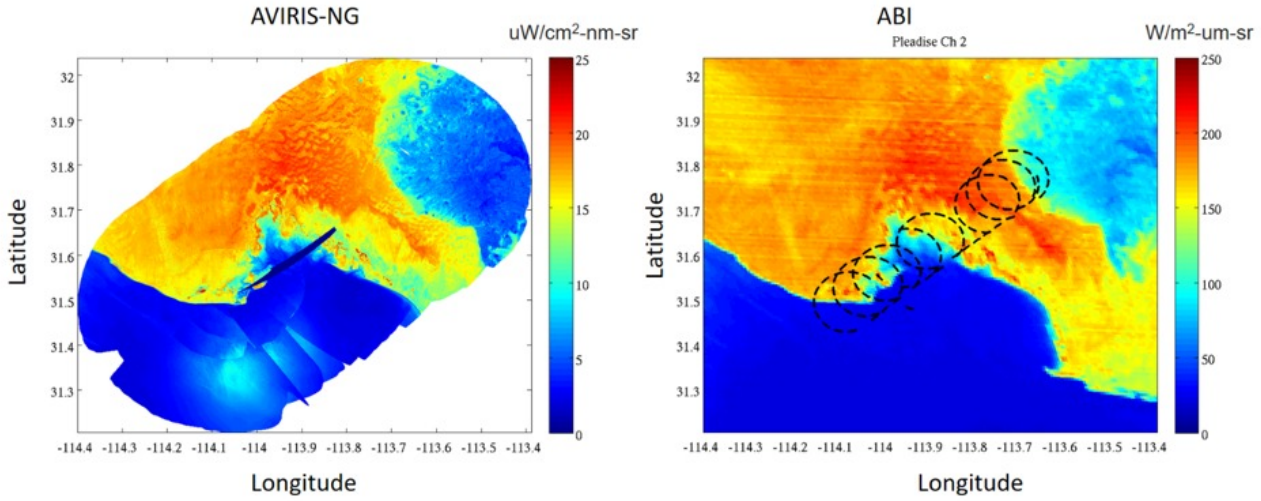

Figure 3: Processed AVIRIS-NG radiance map (left) and ABI observation (right) for GOES-16 ABI CH02 during field campaign on Mar. 28, 2017. Note that the unit for AVIRIS-NG radiance measurement is $\mu W/cm^2$-nm-sr and the radiance unit for ABI measurement is W/m^2-um-sr. The conversion factor is 1 $\mu W/cm^2$-nm-sr = 10 W/m^2-um-sr. So the color map of the two panels are of the same scale.

3. RADIOMETRIC COMPARISON BETWEEN AVIRIS-NG AND ABI MESO SCENE MEASUREMENT

To determine the radiance difference between ABI and AVIRIS-NG for a given ABI RSB channel, it is required to identify optimally matching view geometry samples between ABI and AVIRIS-NG sensor both in time and space. The following ray-matching conditions have been applied in searching for the qualified matching locations.

(1) For the region of interest (RoI), the view angle between ABI line of sight and AVIRIS-NG line of sight should be within 5 degrees. AVIRIS-NG can scan as far as 34 degree off-nadir which made it easy to match the ABI view geometry over the target location during the circular flight paths on Mar. 28, 2017. Since GOES-16 nadir view is fixed at -89.5^o W during field campaign, the view angle of ABI w.r.t. the pixel map of AVIRIS-NG can be readily calculated.
(2) Temporal matching was enforced so that the time difference between ABI observation and AVIRIS-NG measurement over the RoI should be within 30 seconds. The ABI MESO mode scans through the region every 30 seconds and the time stamp of AVIRIS-NG measurement over the RoI can be used to find the closest ABI MESO data in time which constrains the time difference to be within 30 seconds.

There are eight locations in total that satisfy the ray-matching condition. The AVIRIS-NG hyperspectral radiance data have been convolved with the corresponding ABI SRF to derive the radiance for each ABI RSB channel. Due to the higher spatial and spectral resolutions of AVIRIS-NG measurements, the radiance maps over the eight sites show abundant spatial and spectral variations which indicate that the AVIRIS-NG measurements cover variety of land type with substantial features within.

Figure 4-5 show example comparison of measured radiance between ABI-Pleiades and AVIRIS-NG for ABI CH01 and CH02, respectively. The left panels show the comparison between sampled AVIRIS-NG and ABI MESO data over the selected ray-matching site. The AVIRIS-NG data have been convolved with the SRFs of the corresponding ABI RSB channel and ABI MESO data has been sampled into the 5 degree ray-matching region. The ABI and AVIRIS-NG measurements have significantly different spatial resolution. In general, the AVIRIS-NG data capture the fine features within the 5 degree ray-matching region, whereas the ABI data show more averaged feature which matches the pattern in the AVIRIS-NG measurement.

To quantitatively evaluate the radiometric difference between ABI and AVIRIS-NG measurements, mean radiance is calculated by averaging the radiance of the pixels within the ray-matching region. The right panels in Figure 4-5 show the time series of percent difference over eight ray-matching sites between ABI MESO and AVIRIS-NG measurements

for ABI CH01 and CH02, respectively. Over all of the eight ray-matching sites, mean radiance of ABI CH02 is higher than those of AVIRIS-NG.

To further evaluate the mean radiometric bias, Table 1 and Figure 6 summarize the percent radiance bias (ABI-AVIRIS-NG)/AVIRIS-NG [%] by averaging the radiance difference between ABI MESO data and AVIRIS-NG data over the eight ray-matching sites for the five ABI RSB channels. The radiometric bias of ABI CH01 and CH03 are both less than 1%. ABI CH02 and CH05 have positive radiometric bias and ABI CH06 has negative bias, all of which are within 5%. It is noted that during MESO scan, the Sonoran desert region was scanned by a group of ABI detectors, the radiometric biases derived from such comparison only represent the biases of those sampled ABI detectors for a specific RSB channel.

The NSS data collected during the ABI field campaign on Mar. 28, 2017 were analyzed in [9]. Matched co-locations between AVIRIS-NG and ABI NSS data collection on Mar. 28, 2017 have been identified for radiance comparison. The mean radiometric biases determined from MESO and NSS data both show the biases for ABI CH01, Ch03 and CH06 are all within 2%. For ABI CH02, the NSS data show ~7% positive bias. The magnitude of radiometric bias for ABI CH02 is consistent with the bias determined from the independent analyses from GEO-LEO co-location and DCC comparison. The relatively smaller biases determined from the MESO scene for ABI CH02 compared to those derived from the NSS data (all detector validation) can be due to the limited number of ABI detector samples that meet the AVIRIS-NG ray-matching condition (i.e. the MESO approach does not account for all detectors).

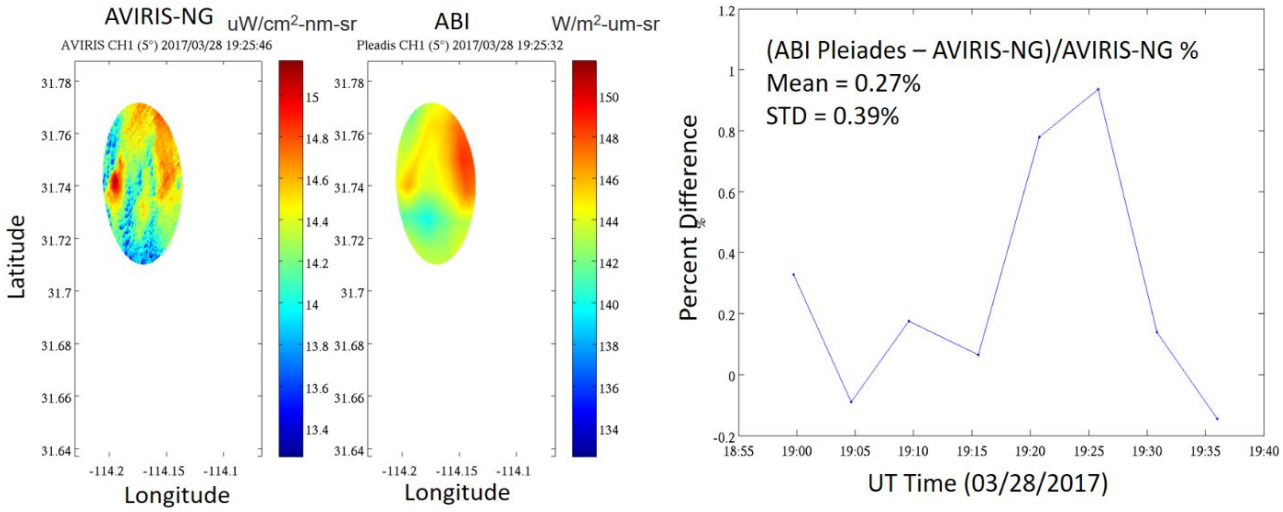

Figure 4: Left: Selected comparison between sampled AVIRIS-NG and ABI MESO data over one ray-matching site (< 5°) during Mar. 28, 2017 for ABI CH01. The AVIRIS-NG data have been convolved with the SRF of ABI CH01. ABI MESO data has been sampled into the 5 degree ray-matching region. Note that the unit for AVIRIS-NG radiance measurement is μW/cm^2-nm-sr and the radiance unit for ABI measurement is W/m^2-um-sr. The conversion factor is 1 μW/cm^2-nm-sr = 10 W/m^2-um-sr. So the color map of the two panels are of the same scale. (Right) Time series of percent difference between the mean radiances of ABI-Pleiades and AVIRIS-NG over the ray-matching sites for ABI CH01.

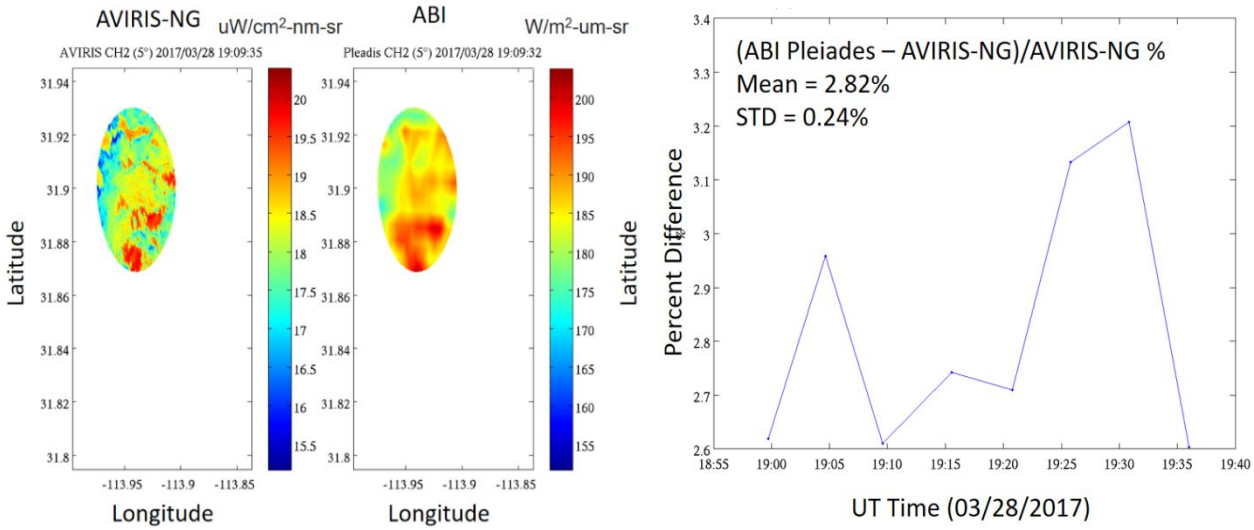

Figure 5: Comparison of measured radiance between ABI-Pleiades and AVIRIS-NG for ABI CH02 during Mar. 28, 2017. The arrangement of panels in this figure is similar to that in Figure 4. ABI radiance over the ray-matching sites is consistently higher than that of AVIRIS-NG.

ABI RSB Channel	CH01	CH02	CH03	CH05	CH06
Bias (%) (ABI Pleiades- AVIRIS-NG)	0.27	2.82	-0.39	2.0	-1.11

Table 1: Tabulated data of the percent difference between ABI-Pleiades and AVIRIS-NG measurements shown in Figure 6.

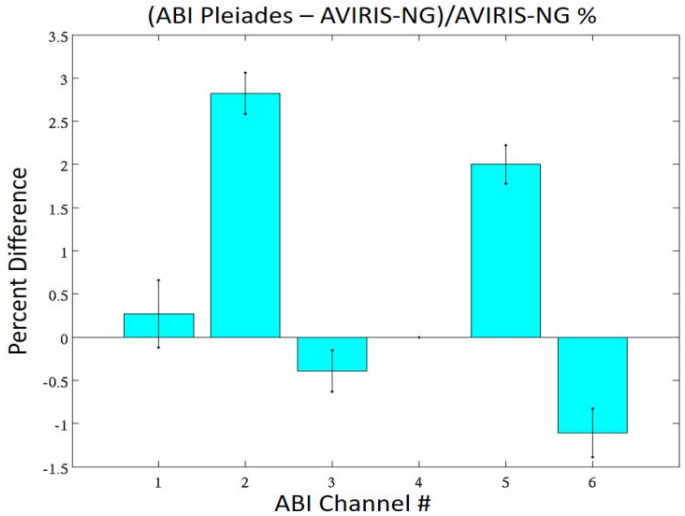

Figure 6: Percent difference and uncertainty between ABI-Pleiades and AVIRIS-NG measurements over MESO scene for ABI RSB channel. Data were derived from field campaign measurements on Mar 28, 2017.

4. REANALYSIS OF NSS FIELD CAMPAIGN DATA FOR ABI RSB CHANNEL DETECTOR UNIFORMITY EVALUATION

4.1 ABI NSS Data Collected during Field Campaign

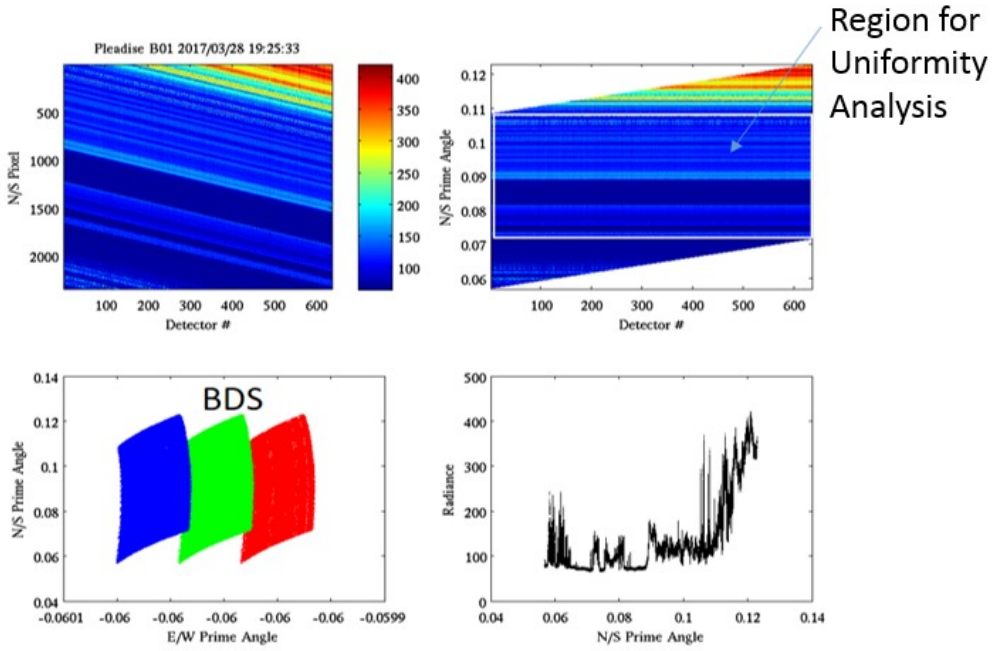

Figure 7: (Top Left) Pixel map of the ABI CH01 NSS data in detector-N/S pixel coordinate. The data were reprocessed by the instrument vendor, *i.e.* Pleiades. (Top Right) NSS data reorganized in the detector-N/S prime angle coordinate. The region for calculating detector-mean radiance L_i is marked as the white rectangle box. (Bottom Left) the E/W and N/S scan angle locations for all of detector during NSS. The color-coding indicates the Best Detector Selection (BDS) identifier for these detectors. The detector array for ABI CH01 has 3 detectors to choose from in each row and the BDS identifier ranges from 1 to 3. (Bottom Right) All-detector-averaged radiance vs. N/S prime angle. Variety of surface features during NSS can be inferred from the large variation of radiances.

Figure 7 shows example of NSS data for ABI CH01 reprocessed by the vendor, *i.e.* Pleiades. The top-left panel shows the measured radiance in the detector-N/S pixel coordinate, *i.e.* pixel map. The slanted stripe indicates sequential scan of the same location by all of the detector during NSS. It is difficult to directly extract data over the same region from the pixel map. Therefore, NSS data were reorganized in the coordinate of detector-N/S prime angle, *i.e.* the N/S scan angle (see right panel in Figure 2). Such coordinate transformation enables the detector-uniformity evaluation. To minimize the noise in the data and increase the sample size, the NSS data within 96% of the common N/S prime angle range for all of the detector are collected. These data are averaged over the same N/S prime angle range for each detector and the resulting mean radiance is labeled as $\overline{L_i}$ for detector i which will be used to evaluate detector uniformity.

The bottom left panel shows the E/W and N/S scan angle locations for all of detectors during NSS. The locations are color-coded with the ABI Best Detector Selection (BDS) identifier. Since the detector array for each ABI channel has multi-columns, one best detector was selected for each row of ABI detector and such selected detector is labeled with the BDS identifier. For ABI CH01, there are three columns in the detector array and the BDS identifier ranging from 1 to 3. It can be seen that there are small differences in the E/W scan angle locations among the detectors with different BDS identifier.

4.2 ABI RSB Solar Calibration Algorithms

The radiance observed by GOES-16 ABI RSB channel viewing the earth scene is determined from the measured counts (C) of the earth view (*ev*) and the space view (*sv*) as follows

$$< L_{ev} >= \frac{M\Delta C_{ev}+Q\Delta C_{ev}^2}{\rho_{NS}^{ev}\rho_{EW}^{ev}}, \quad (1)$$

where $< L_{ev}>$ is the band-averaged spectral radiance for the scene in the earth view, *i.e.*, W/(m2-sr-μm) for the RSB. ΔC_{ev} is the count difference between Earth view and space view, *i.e.* $\Delta C_{ev} = C_{ev} - C_{sv}$. M and Q are the linear and quadratic coefficients, respectively. The quadratic coefficient Q is first determined pre-launch per band and per detector element and later updated post-launch. The linear coefficient M for RSB is determined on-orbit viewing the Solar Calibration Target (SCT), which is a solar diffuser. The $\rho_{NS}^{ev}, \rho_{EW}^{ev}$ are the reflectance of the East/West and North/South scan mirrors respectively, when viewing Earth scene.

This study reprocessed the NSS data using different versions of detector linear (M) and nonlinear calibration factor (Q), and evaluate the radiometric quality changes due to corresponding changes in the ABI RSB radiometric calibration. In doing so, the GRATDAT software was used to decompress the L0 data of NSS collection into raw detector counts. *i.e.* L1A data. This paper uses the NOAA/STAR L1A-to-L1Alpha conversion tool to reprocess the NSS L1A data to radiance data for any given pair of linear and nonlinear calibration factor LUT that were derived from different versions of solar calibration for ABI RSB.

The following calibration algorithms have been investigated in this paper through reanalysis of the NSS data.

(A) Pleiades: Solar calibration to derive detector gain factor and processing the NSS raw data to radiance data were both performed by the ABI vendor. The solar calibration was performed with nonlinear calibration factor Q being set as 0.

(B) STAR/CWG: Reanalysis of NSS data using the calibration coefficients derived from Mar. 16, 2017 solar diffuser data with the solar calibration model developed at NOAA/STAR. Such reprocessing of NSS data is performed with the CWG L1A-to-L1Alpha conversion tool. This model uses the prelaunch nonlinear calibration factor Q LUT in both the solar calibration and the L1A-to-L1Alpha conversion.

(C) Implementation of Q-Scaling scheme in Solar Calibration
It was noticed that the striping in the ABI imageries of RSB channel can be caused by the amplified effect of the nonlinear Q factor used in the solar calibration. Therefore, the Q-scaling scheme was proposed to scale the nonlinear Q factor down by the corresponding integration time factor for solar diffuser view, *i.e.* 9, in the solar calibration. When applying the derived linear gain factor M into Eq. 1, full-Q was used in converting the earth view data into the L1Alpha radiance data. In addition, new nonlinear Q LUT was developed together with the Q-scaling scheme by ABI ground system (GS) to mitigate the striping problem for ABI CH01, CH02 and CH03.

4.3 Results of NSS Data Reanalysis

In this section, the reanalysis result of ABI CH01 NSS data is shown as an example. Figure 8 shows the relative mean-radiance RL (%) differences among detectors derived from the reprocessed radiance data of three calibration models (listed in section 4.2) for ABI CH01. First, the mean-radiance $\overline{L_i}$ for detector i is calculated by averaging the detector radiance over the same N/S prime angle range (see right panel in Figure 7 for illustration of the N/S prime angle range). The relative mean-radiance difference for detector i=1, N is defined as RL_i (%) = $(\frac{\overline{L_i}}{\sum_1^N \overline{L_i}/N}-1)\times 100$, which is the key parameter used to assess the detector uniformity for each ABI channel.

In Figure 8, the color-coding for scattered points in each panel indicates the corresponding BDS identifier for each detector. Apparent distribution of RL according to BDS level can be identified which might be due to the slight difference in the E/W scan-angle location of these detectors. Several key points can be inferred from the comparison in Figure 8.

(a) Overall distribution of RL derived from Model A is similar to that of Model B.

(b) The Q-scaling paired with new Q-LUT (Model C) significantly reduce the detector-to-detector spread. This can be inferred from the reduction in the standard deviation of RL, *i.e.* σ_{RL}, for each BDS group. For example, σ_{RL}=

1.11% to 1.22% for Model A; σ_{RL}= 1.13% to 1.23% for Model B; and σ_{RL}= 0.17% to 0.3% for Model C with Q-scaling and new Q-LUT. The significant (> 4 times) reduction in σ_{RL} indicates that the detector uniformity has been largely enhanced with Model C1.

(c) Comparing the *RL* of Model A and Model C, it can be seen that the outliers (marked with red oval) with large negative *RL* have been removed. This indicates that the de-striping algorithm implemented in Model C is successful.

(d) Model C still has a residual rising slope of ~1% across detectors. It is worth of pointing out that the ability of identifying the residual ~1% slope across detectors with the NSS data can greatly help validate the prelaunch solar diffuser BRDF LUT used in the solar calibration.

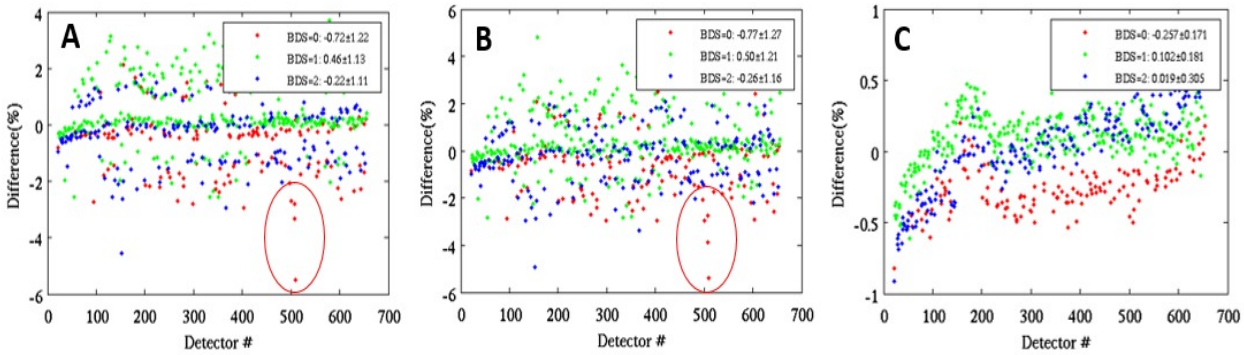

Figure 8: Detector-uniformity analysis with relative mean-radiance difference *RL* (%) among detectors for ABI CH01 as derived from three calibration algorithms: (Model A) Reprocessed by vendor (Pleiades version); (Model B) Reprocessed with prelaunch *Q* LUT and gain *M* derived from NOAA/STAR implementation of solar calibration; (Model C) Reprocessed with updated Q LUT in 2018 and gain *M* derived from NOAA/STAR implementation of Q-scaling solar calibration. The legend in each panel shows the mean and standard deviation of *RL* grouped according to BDS. The overall standard deviation for all detector is marked at the top of each panel.

5. SUMMARY

In this paper, the radiometric differences between ABI-Pleiades MESO and AVIRIS-NG measurements over co-located targets in Sonoran desert region on Mar. 28, 2017 are summarized. In comparison with AVIRIS-NG measurements, the mean radiometric biases for ABI CH01, Ch03 and CH06 determined from MESO and NSS data are all within 2%. The mean bias level of ABI CH05 is about 2-3%. For ABI CH02, the MESO data comparison shows ~2.8% positive bias and the NSS comparison in [9] shows ~7% positive bias, which is more consistent with the bias determined from the independent analyses with GEO-LEO co-location and DCC data comparison. The difference for the ABI CH02 biases determined by the MESO versus NSS data can be due to much less number of detector samples that satisfies the ray-matching condition in ABI MESO collection than those in NSS collection. This will be further verified by reprocessing the L1b data to locate the actual detectors used for comparison to the NSS-generated detector-uniformity results.By reprocessing the ABI NSS data with different calibration algorithms, this paper also demonstrated that the ABI NSS data enabled quantitative evaluation of the detector uniformity improvements due to the implementation of the Q-scaling scheme and new Q-LUT in solar calibration.

ACKNOWLEDGEMENT

The manuscript contents are solely the opinions of the authors and do not constitute a statement of policy, decision, or position on behalf of NOAA or the U.S. government.

REFERENCES

[1] Kalluri, S., Alcala, C., Carr, J., Griffith, P., Lebair, W., Lindsey, D., Race, R., Wu, X., and Zierk, S., "From Photons to Pixels: Processing Data from the Advanced Baseline Imager," Remote Sens. 10(177), (2018).

[2] Yu, F., Wu, X., Shao, X., Efremova, B., Yoo, H., Qian, H., and Iacovazzi, B., "Early radiometric calibration performances of GOES-16 Advanced Baseline Imager," Proc. SPIE Earth Observing Systems XXII 104020, (2017).

[3] Yu, F., Shao, X., Wu, X., Kondratovich, V., and Li, Z., "Validation of early GOES-16 ABI on-orbit geometrical calibration accuracy using SNO method," Proc SPIE Earth Observing Systems XXII 10402, (2017).

[4] Padula, P., Goodman, S., Pearlman, A., and Cao C., "GOES-R Advanced Baseline Imager (ABI) and Geostationary Lightning Mapper (GLM) Calibration/Validation From A Field Campaign Perspective," Proc. IGARSS, New GEO/LEO Mission Advanced Imagery Products: Optical Sensor Calibration and Applications II MO4.L8.3, (2017).

[5] Padula, F., Pearlman, A., Cao, C., and Goodman, S., "Towards post-launch validation of GOES-R ABI SI traceability with high-altitude aircraft, small near surface UAS, and satellite reference measurements," Proc. SPIE 9972, Earth Observing Systems XXI 99720, (2016).

[6] Padula. F., Pearlman, A. J., Goodman, S. J., Efremova, B.,McCorkel, J., Pogorzala, D., Shao, X. Casey, J., Bartlett, B., Uprety, S., and Cao, C., "GOES-R Post-Launch Airborne Science Field Campaign: An Independent Validation of NOAA's Next Generation Geostationary Imager." AMS Annual Conf., (2018).

[7] Hamlin, L., Green, R., Mouroulis, P., Eastwood, M., Wilson, D., Dudik, M., and Paine, C., "Imaging Spectrometer Science Measurements for Terrestrial Ecology: AVIRIS and New Developments," Aerospace Conference, IEEE, https://doi.org/10.1109/AERO.2011.5747395, (2011).

[8] Thompson, D. R., Roberts, D. A., Gao, B. C., Green, R. O., Guild, L., Hayashi, K., Kudela, R., and Palacios, S., "Atmospheric Correction with the Bayesian Empirical Line," Optics Express 24, 2134 (2016).

[9] Bartlett, B., Casey, J., Padula, F., Pearlman, A., Pogorzala, D., and Cao, C., "Independent validation of the advanced baseline imager (ABI) on NOAA's GOES-16: Post-launch ABI airborne science field campaign results," Proc. SPIE Earth Observing Systems XXIII 10764, (2018).